

AUTOMATED AND RISK-AWARE ENGINE CONTROL CALIBRATION USING CONSTRAINED BAYESIAN OPTIMIZATION

PREPRINT, COMPILED MARCH 27, 2025

Maarten Vlaswinkel^{1,*}, Duarte Antunes¹, and Frank Willems^{1,2}

¹Control Systems Technology, Eindhoven University of Technology, Eindhoven, The Netherlands

²Powertrains Department, TNO Mobility & Built Environment, Helmond, The Netherlands

ABSTRACT

Decarbonization of the transport sector sets increasingly strict demands to maximize thermal efficiency and minimize greenhouse gas emissions of Internal Combustion Engines. This has led to complex engines with a surge in the number of corresponding tuneable parameters in actuator set points and control settings. Automated calibration is therefore essential to keep development time and costs at acceptable levels. In this work, an innovative self-learning calibration method is presented based on in-cylinder pressure curve shaping. This method combines Principal Component Decomposition with constrained Bayesian Optimization. To realize maximal thermal engine efficiency, the optimization problem aims at minimizing the difference between the actual in-cylinder pressure curve and an Idealized Thermodynamic Cycle. By continuously updating a Gaussian Process Regression model of the pressure's Principal Components weights using measurements of the actual operating conditions, the mean in-cylinder pressure curve as well as its uncertainty bounds are learned. This information drives the optimization of calibration parameters, which are automatically adapted while dealing with the risks and uncertainties associated with operational safety and combustion stability. This data-driven method does not require prior knowledge of the system. The proposed method is successfully demonstrated in simulation using a Reactivity Controlled Compression Ignition engine model. The difference between the Gross Indicated Efficiency of the optimal solution found and the true optimum is 0.017%. For this complex engine, the optimal solution was found after 64.4 s, which is relatively fast compared to conventional calibration methods.

Keywords: Machine Learning; Bayesian Optimisation; Gaussian Process Regression; Principle Component Decomposition; Auto-calibration

1 INTRODUCTION

The current demand on increasing the thermal efficiency and decreasing the emissions of Internal Combustion Engines (ICEs) has led to the development of more advanced combustion concepts (Adam B. Dempsey and Reitz, 2014). Reactivity Controlled Compression Ignition (RCCI) is one of the considered concepts (Kokjohn et al., 2011) for ultra efficient and clean combustion. RCCI combustion is characterised by the use of two fuels. A low-reactivity fuel (e.g., E85) and a high-reactivity fuel (e.g., Diesel) are mixed in the combustion chamber. This makes it possible to control the reactivity of the fuel, thus giving control over the ignition timing.

The need to meet current and future increasingly strict emission legislations has led to an increase in the number of subsystems and actuators (Willems, 2018; Norouzi et al., 2021). This leads to an increase in the number of tuneable actuator setpoints, references and feedback control parameters requiring tuning during ICE control calibration. As the number of parameters increase, the time and complexity of the calibration process will rise to unacceptable levels. During calibration the settings for the parameters are determined that make sure that the engine meets pre-described performance targets. As a result, this will make ICE calibration a more important part of ICE development. Developing novel calibration methods is a vital step to keep future and more advanced ICEs commercially viable (Paykani et al., 2021). In this work, the focus will be on

the calibration of the fuel actuator settings related to timing and quantity of injection.

1.1 Time Efficient Engine Calibration

Calibration approaches have been proposed using model-based methods (e.g., Grasreiner et al. (2017)) or using a predetermined Design of Experiments (DOE) (e.g., Motlagh et al. (2020); Xia et al. (2020); Willems et al. (2021); Biswas et al. (2022); Moradi et al. (2022)). Model-based methods use a validated combustion model to determine optimal parameter settings. These models are validated using experimental data. The quality of calibration is greatly determined by the quality of the model. DOE methods treat the engine as a black-box system and use no, or only a small amount, of prior system knowledge. DOE is used as a tool to determine key system behaviour in minimal testing time. It separates the collection of engine data and the process of determining the optimal actuator setpoints. The data collected using the DOE is used as an input to a regression tool. Xia et al. (2020) was able to include cycle-to-cycle variations into the calibration problem.

Developing an engine model or determining the DOE are not trivial tasks. For experimental combustion concepts the safe operating regions are often unknown. Therefore, selecting appropriate actuator ranges is challenging and requires expertise. Simultaneous collecting data and the optimization of the ICE performance can solve this challenge. Bayesian Optimisation

(BO) is seen as a more adaptive and iterative method for DOE (Greenhill et al., 2020). The system is treated as a black-box, thus no prior knowledge of the system is required. For ICEs, the safe operating domain is not linked to actuator ranges. Therefore, the BO approach should be aware of possible risky behaviour which has not been tackled in the literature, to the best of the authors knowledge.

1.2 Shaping of the In-cylinder Pressure

In this paper, an automated, risk-aware calibration method is presented. This method requires no prior knowledge of the system. The method is able to deal with unknown constraint boundaries and cycle-to-cycle variations. It extends upon the Principal Component Decomposition (PCD) and Gaussian Process Regression (GPR) based in-cylinder pressure model presented in Vlaswinkel and Willems (2024) and the Idealised Thermodynamic Cycle (ITC) based cost function presented in Vlaswinkel and Willems (2023). The in-cylinder pressure model will predict the in-cylinder pressure between Intake Valve Close (IVC) and Exhaust Valve Open (EVO) given actuator setpoints. The ITC based cost function generates an idealised in-cylinder pressure profile. The calibration problem is reformulated into a probabilistic framework using a constrained BO approach.

1.3 Outline of this Paper

This work is organized as follows. In Section 2, a description of the system and calibration problem are presented. Section 3 presents the automated risk-aware calibration method. Sections 3.1 until 3.3 give a summary of the work presented in Vlaswinkel and Willems (2023) and Vlaswinkel and Willems (2024). In Sections 3.5 until 3.7, the new contributions to the calibration method are presented. Section 4 discusses the observed behaviour of the method and a comparison is made between different acquisition functions using a simulated RCCI engine fuelled with Diesel and E85.

2 PROBLEM DESCRIPTION

The main objective of this work is to maximize thermal efficiency for a requested power output, while respecting bounds on mechanical stresses and combustion stability, by automated calibration of the engine control settings.

2.1 System Description

In this research, the optimization of the fuel settings of a single cylinder RCCI engine is studied to demonstrate the potential of the novel automated control calibration method. This engine is equipped with a standard Direct Injection (DI) injector, which injects Diesel directly into the cylinders. The actuation signals of the DI injector consist of the start-of-injection SOI_{DI} and the injected mass of Diesel m_{DI} . For RCCI research, an additional injector is installed in the intake for Port Fuel Injection (PFI) of E85. The actuation signal of the port fuel injector consists of the mass of injected E85 m_{PFI} . The start-of-injection of the port fuel injector is kept constant at -320 Crank Angle Degrees after Top Dead Center (CADaTDC). Note that we only

consider single pulse DI and PFI fuel injection. The cylinder intake and exhaust conditions associated with the air path s_{air} , such as Exhaust Gas Recirculation (EGR) ratio, intake and exhaust manifold pressure, and intake manifold temperature are kept constant in this work. The engine specifications and the operating conditions studied are listed in Table 1. The operating conditions are chosen to align with the model developed in Vlaswinkel and Willems (2024).

2.2 Problem Formulation

During the calibration of the combustion process, the fuelling parameters s_{fuel} are used to maximise the gross indicated efficiency GIE defined as

$$GIE(s_{fuel}, s_{air}) = \frac{\int_{\Theta} p(\theta, s_{fuel}, s_{air}) dV(\theta)}{Q_{fuel}}, \quad (1)$$

where $p(\theta)$ is the in-cylinder pressure over the crank-angle position $\theta \in \Theta$, $\Theta = [-180, 180]$ CADaTDC, $V(\theta)$ is the cylinder volume, and Q_{fuel} is the total fuel energy. For the RCCI engine studied, three fuelling parameters s_{fuel} are defined. First, the total fuel energy

$$Q_{fuel} = m_{PFI}LHV_{PFI} + m_{DI}LHV_{DI} \quad (2)$$

with m_{PFI} and m_{DI} the injected fuel mass and LHV_{PFI} and LHV_{DI} the lower-heating value of the Port Fuel Injection (PFI) and Direct Injection (DI) fuels, respectively, is considered. Second, we use the energy-based blend ratio

$$BR = \frac{m_{PFI}LHV_{PFI}}{Q_{fuel}}. \quad (3)$$

And third, the start-of-injection of the directly injected fuel SOI_{DI} is used.

Engine operation is typically defined by engine speed and power output. The gross Indicated Mean Effective Pressure $IMEP_g$ is a measure for the provided piston work during the power stroke and is given by

$$IMEP_g(s_{fuel}, s_{air}) = \frac{\int_{\Theta} p(\theta, s_{fuel}, s_{air}) dV(\theta)}{V_d} \quad (4)$$

with displacement volume V_d . For a meaningful comparison of results, this value is kept constant during optimisation and should meet the driver's request $IMEP_{g,req}$. The engine speed is kept constant. To ensure safety and stable combustion, the optimisation process must respect the limits of the maximum in-cylinder pressure p_{ub} , the increase rate of the maximum pressure dp_{ub} and the coefficient of variation

$$cov(IMEP_g) = \frac{\sigma_{IMEP_g}}{\mu_{IMEP_g}} \quad (5)$$

with μ_{IMEP_g} and σ_{IMEP_g} the mean and standard deviation of $IMEP_g$, respectively.

Table 1: Properties of the simulated single cylinder Reactivity Controlled Compression Ignition engine

Parameter	Value
PFI fuel	E85
DI fuel	Diesel
Compression ratio	17.2
Bore	130 mm
Stroke	162 mm
Displacement volume V_d	2200 mm ³
Engine speed	1200 rpm
Intake manifold pressure	1 bar
Intake manifold temperature	45 °C
EGR ratio	0.2
DI common-rail pressure	600 bar

In summary, the engine optimization problem can be formulated as:

$$s_{\text{fuel}}^* = \arg \max_{s_{\text{fuel}} \in \mathcal{S}_{\text{fuel}}} \text{GIE}(s_{\text{fuel}}, s_{\text{air}}), \quad (6a)$$

$$\text{s.t. } \text{IMEP}_g(s_{\text{fuel}}, s_{\text{air}}) = \text{IMEP}_{g,\text{req}}, \quad (6b)$$

$$\text{cov}(\text{IMEP}_g(s_{\text{fuel}}, s_{\text{air}})) < \left[\text{cov}(\text{IMEP}_g(s_{\text{fuel}}, s_{\text{air}})) \right]_{\text{ub}}, \quad (6c)$$

$$\max_{\theta} (p(\theta, s_{\text{fuel}}, s_{\text{air}})) < p_{\text{ub}}, \quad (6d)$$

$$\max_{\theta} \left(\left. \frac{\partial p(s_{\text{fuel}}, s_{\text{air}})}{\partial \theta} \right|_{\theta} \right) < dp_{\text{ub}}. \quad (6e)$$

where $s_{\text{fuel}} = [Q_{\text{fuel}}, \text{BR}, \text{SOI}_{\text{DI}}]^T$ and s_{fuel}^* the optimal fuel parameters which solves (6). The work generated by combustion is given by (6b), the combustion stability limit by (6c) and the safety constraints by (6d)-(6e) to limit mechanical stresses.

The system is treated like a black box. At the beginning of the optimization process, only an initial s_{fuel} must be provided that meets the combustion stability and safety constraints of (6c)-(6e).

3 BAYESIAN OPTIMISATION FRAMEWORK

In this section, the Bayesian Optimisation (BO) framework is presented that solves (6) without the need for prior knowledge of the engine. This innovative framework is schematically represented in Figure 1 and consists of four essential components:

1. Next-cycle IMEP_g control to realize the requested engine load by the driver;
2. Targeted Ideal Thermodynamic Cycle (ITC);
3. Learning a model of the weights w associated with the Principal Components of the observed in-cylinder pressure;
4. Constrained Bayesian Optimization to determine the fuel optimal s_{fuel}^* .

Figure 1a gives an overview of the interaction between the different components in the framework. The BO is driven by a Principal Component Decomposition (PCD) of the observed in-cylinder pressure and a Gaussian Process Regression (GPR) model \mathcal{M}_w that maps BR and SOI_{DI} to the Principal Component (PC) weights w . To guarantee a power output equal to the driver's demand, the IMEP_g is controlled outside the optimization loop by a next-cycle combustion controller using Q_{fuel} . To reduce the computation time of the GPR model, the collected data is summarized, as shown in Figure 1b. After convergence of IMEP_g , the buffer will collect the PC weights of the last n combustion cycles. The mean and standard deviation of these collected PC weights, i.e. M_{wi} and Σ_{wi} respectively, are added to the GPR model. This continuous update of the GPR model is also referred to as the self-learning part of the framework. Figure 1c shows the process of selecting a new actuator settings candidate. After new data has been added to the GPR model, a new solution is found for BR and SOI_{DI} . An acquisition function is optimized using the current information in the GPR model while respecting the constraints. The optimization is carried out by a Particle Swarm Optimization (PSO). After convergence of the PSO, the optimal candidate that solves (6) given the current information about the system is found and is applied to the system. The main components of the BO framework will be discussed in more detail in the following sections.

3.1 Principle Component Decomposition of In-Cylinder Pressure

The current section is based upon the work described in Vlaswinkel and Willems (2024). The sampled in-cylinder pressure $p(\theta, s_{\text{fuel}}, p_{\text{im}})$ at crank angle $\theta \in \{-180, -180 + \Delta\text{CA}, \dots, 180 - \Delta\text{CA}, 180\}$ CADaTDC with ΔCA the crank angle resolution is decomposed as

$$p(\theta, s_{\text{fuel}}, p_{\text{im}}) = p_{\text{mot}}(\theta, p_{\text{im}}) + w(s_{\text{fuel}})^T f(\theta), \quad (7)$$

where $w(s_{\text{fuel}}) \in \mathbb{R}^{n_{\text{PC}}}$ is a vector of weights and $f(\theta) \in \mathbb{R}^{n_{\text{PC}}}$ is the vector of PCs with n_{PC} the number of PCs. The motored pressure is modelled by an adiabatic process and is given by

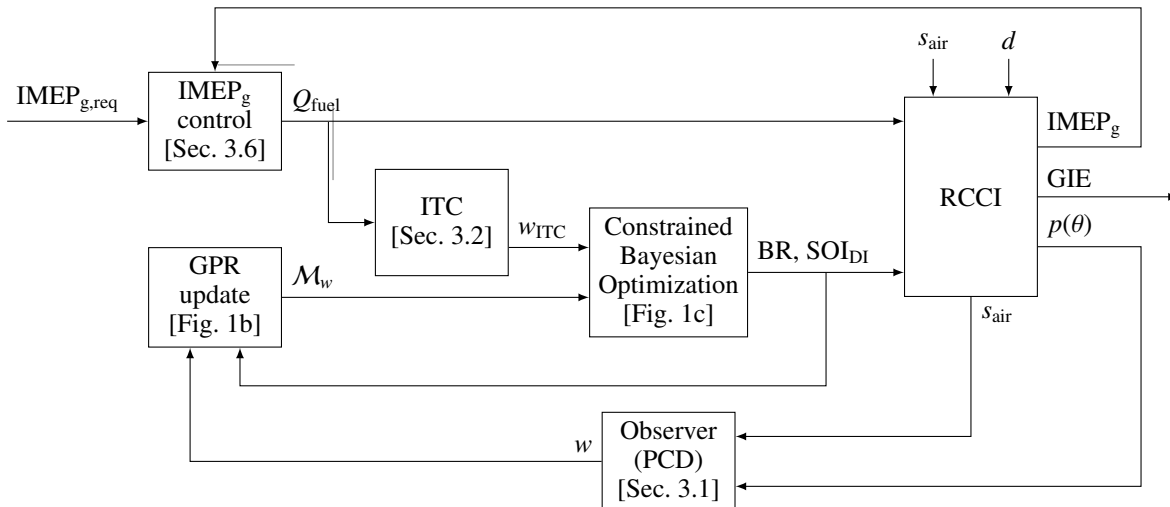
$$p_{\text{mot}}(\theta, p_{\text{im}}) = p_{\text{im}} \left(\frac{V(-180 \text{ CADaTDC})}{V(\theta)} \right)^{\kappa} \quad (8)$$

with cylinder volume $V(\theta)$ and specific heat ratio κ . In the vectors $w(s_{\text{fuel}})$ and $f(\theta)$, the i th element is related to the i th PC. The in-cylinder condition $s_{\text{fuel}} \in \mathcal{S}$ are in the set \mathcal{S} spanning the modelled operation domain. It is assumed that the in-cylinder pressure during the intake stroke is equal to the intake manifold pressure p_{im} .

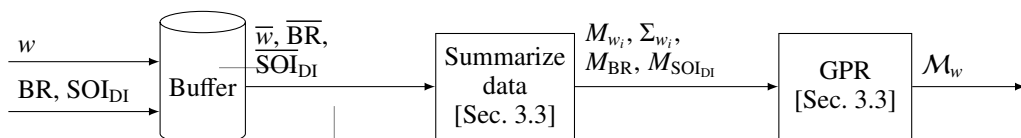
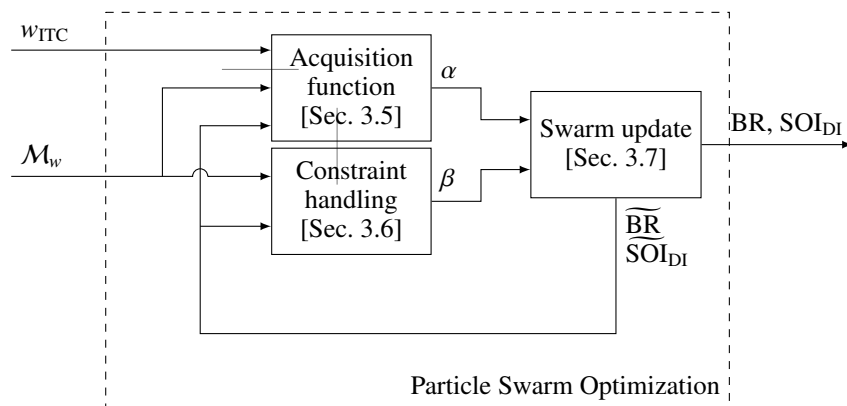
The eigenvalue method is used to compute the PCs. The $n_{\text{train}} \cdot n_{\text{cyc}}$ in-cylinder pressures $p(\theta, s_{\text{fuel}}^*)$ contained in the training set are used, where n_{train} is the number of experiments in the training dataset and n_{cyc} the number of combustion cycles within an experiment. The fuel setpoints for PC training are denoted by $s_{\text{fuel}}^* \in \mathcal{S}^* \subset \mathcal{S}$. The vector F_i is the i th unit eigenvector of the matrix PP^T where $P \in \mathbb{R}^{n_{\text{CA}} \times n_{\text{train}} n_{\text{cyc}}}$ with n_{CA} the number of crank angle values. The elements in matrix P are defined as

$$[P]_{ab} := p(\theta_a, s_{\text{fuel},b}^*) - p_{\text{mot}}(\theta_a, s_{\text{fuel},b}^*), \quad (9)$$

such that the a th row of P contains the values of the in-cylinder pressure at the a th crank angle for all $s_{\text{fuel}}^* \in \mathcal{S}^*$ and the b th



(a) High-level overview of the Bayesian Optimization framework


 (b) Updating of Gaussian Process Regression model; runs after n combustion cycles after IMEP_g has converged


(c) Bayesian optimization approach; runs after and update of the Gaussian Process Regression (GPR) update block until the Particle Swarm Optimization (PSO) has converged

Figure 1: Schematic representation of the optimisation approach presented in this work.

column of P contains the full in-cylinder pressure at all $\theta \in \{-180, -180 + \Delta CA, \dots, 180 - \Delta CA, 180\}$ CADaTDC for the b th s_{ICC}^* . The i th PC is defined as

$$f_i(\theta_a) = [F_i]_a. \quad (10)$$

Using these PCs, the weight related to the i th PC is given by

$$w_i(s_{\text{fuel}}) = P(s_{\text{fuel}})F_i, \quad (11)$$

where $[P(s_{\text{fuel}})]_a = p(\theta_a, s_{\text{fuel}}) - p_{\text{mot}}(\theta_a, p_{\text{im}})$.

The training set generates a single set of PCs. These PCs are ordered by the amount of variation in the dataset it captures, where $i = 1$ is the PC that captures the largest variation. In Vlaswinkel and Willems (2024), it was determined that the first 8 PCs are required to properly describe the in-cylinder pressure using PCD.

3.2 Idealised Thermodynamic Cycle Tracking

Using the PCD from the previous section, we introduce an efficiency-based performance measure, which determines the energy loss compared to a pre-defined ideal in-cylinder pressure curve. For more details, the reader is referred to Vlaswinkel and Willems (2023).

3.2.1 Energy Loss Criterion

The total amount of energy has to be conserved during combustion. This means

$$W_{\text{ind,g}} = \text{IMEP}_g V_d = Q_{\text{fuel}} + Q_{\text{loss}}, \quad (12)$$

where $W_{\text{ind,g}} = \int p dV$ is the gross indicated work applied to the piston, V_d is the displacement volume of the cylinder, Q_{loss} are

the total energy losses and Q_{fuel} is the total fuel energy as defined in (2). These losses are divided into two parts: 1) the energy loss obtained when running an Idealised Thermodynamic Cycle (ITC) and 2) the additionally energy losses Q_{NITC} associated with the actual non-ITC. This can be written as

$$Q_{\text{loss}} = (1 - \eta_{\text{ITC}})Q_{\text{fuel}} + Q_{\text{NITC}}, \quad (13)$$

where η_{ITC} is the indicated fuel conversion efficiency of the ITC process. Substituting (13) into (12) gives

$$Q_{\text{NITC}} = W_{\text{ind,g}} - \eta_{\text{ITC}}Q_{\text{fuel}}. \quad (14)$$

The Gross Indicated Efficiency (GIE) is maximized when Q_{NITC} is as close to zero as possible. This is done by defining the cost function

$$J = Q_{\text{NITC}}^2. \quad (15)$$

Given the PCD of a measured in-cylinder pressure curve $p(\theta)$ and of a pressure curve $p_{\text{ITC}}(\theta)$ associated with ITC, (15) can be rewritten using (7):

$$\begin{aligned} J &= \left(\int_{\Theta} w(s_{\text{fuel}}, s_{\text{air}})^{\top} f(\theta) + p_{\text{mot}}(\theta, p_{\text{im}}) + \right. \\ &\quad \left. \epsilon(\theta) dV - \int_{\Theta} w_{\text{ITC}}^{\top} f(\theta) + p_{\text{mot}}(\theta, p_{\text{im}}) + \right. \\ &\quad \left. \epsilon_{\text{ITC}}(\theta) dV \right)^2, \\ &= (w(s_{\text{fuel}}, s_{\text{air}}) - w_{\text{ITC}})^{\top} Z_1 (w(s_{\text{fuel}}, s_{\text{air}}) - w_{\text{ITC}}) + \\ &\quad 2(w(s_{\text{fuel}}, s_{\text{air}}) - w_{\text{ITC}})^{\top} Z_2 + Z_3 \end{aligned} \quad (16)$$

with

$$\begin{aligned} Z_1 &= \iint_{\Theta} f(\theta_1) f^{\top}(\theta_2) dV(\theta_1) dV(\theta_2), \\ Z_2 &= \iint_{\Theta} f(\theta_1) (\epsilon(\theta_2) - \epsilon_{\text{ITC}}(\theta_2)) dV(\theta_1) dV(\theta_2) \end{aligned}$$

and

$$Z_3 = \iint_{\Theta} (\epsilon(\theta_1) - \epsilon_{\text{ITC}}(\theta_1)) (\epsilon(\theta_2) - \epsilon_{\text{ITC}}(\theta_2)) dV(\theta_1) dV(\theta_2).$$

The weights w and w_{ITC} of the measured and ITC curves are determined such that $\int_{\Theta} \epsilon(\theta)^2 dV(\theta)$ and $\int_{\Theta} \epsilon_{\text{ITC}}(\theta)^2 dV(\theta)$ are minimised, respectively. When enough PCs are used these terms will approach 0; therefore, it can be assumed that $Z_2 \approx 0$ and $Z_3 \approx 0$. This reduces (16) to the following energy loss criterion:

$$J \approx J_{\text{ITC}} = (w(s_{\text{fuel}}, s_{\text{air}}) - w_{\text{ITC}}(s_{\text{fuel}}, s_{\text{air}}))^{\top} \cdot Z_1 (w(s_{\text{fuel}}, s_{\text{air}}) - w_{\text{ITC}}(s_{\text{fuel}}, s_{\text{air}})). \quad (17)$$

3.2.2 Otto Cycle Pressure Model

In this article, the Otto cycle is used as ITC, because it promises the highest thermal efficiency over a large operating range (Heywood, 2018). It is a combination of two isentropic and two isochoric processes. It can be fully described by the total fuel energy Q_{fuel} , the pressure at the start of the compression stroke p_{low} , cylinder volume $V(\theta)$, and temperature and composition dependent specific heat ratio κ . The in-cylinder pressure corresponding to the Otto cycle is given by:

$$p_{\text{ITC}}(\theta, Q_{\text{fuel}}, p_{\text{im}}) = \begin{cases} p_{\text{low}} \left(\frac{V(-180\text{CAD})}{V(\theta)} \right)^{\kappa}, & \text{if } \theta \in \Theta_c, \\ p_{\text{high}} \left(\frac{V(0\text{CAD})}{V(\theta)} \right)^{\kappa}, & \text{if } \theta \in \Theta_e \end{cases} \quad (18)$$

with $\Theta_c = [-180, 0]$ CADaTDC, $\Theta_e = [0, 180]$ CADaTDC,

$$p_{\text{high}} = \frac{\eta_{\text{ITC}} Q_{\text{fuel}} - \int_{-180\text{CAD}}^{0\text{CAD}} p_{\text{ITC}}(\theta, Q_{\text{fuel}}) dV}{V^{\kappa}(0\text{CAD}) \int_{-180\text{CAD}}^{0\text{CAD}} V^{-\kappa}(\theta) dV(\theta)}$$

and thermal efficiency of the Otto cycle η_{ITC} is given by

$$\eta_{\text{ITC}} = 1 - \frac{1}{r^{\kappa-1}} \quad (19)$$

with the compression ratio $r = \max(V) \min(V)^{-1}$. Using (19), it is found that the thermal efficiency increases when κ increases. Note that the air-path conditions determine p_{low} and κ .

3.3 Gaussian Process Regression Prediction Model

Gaussian Process Regression (GPR) is used to predict the behavior of each component of $w(s_{\text{fuel}})$ over the entire operation domain \mathcal{S} . To include cycle-to-cycle variations in the in-cylinder pressure, $w(s_{\text{fuel}})$ is described by a stochastic process as

$$w(s_{\text{fuel}}) := \mathcal{N}(\hat{w}(s_{\text{fuel}}), \hat{W}(s_{\text{fuel}})) \quad (20)$$

with mean $\hat{w}(s_{\text{fuel}}) := \mathbb{E}[w(s_{\text{fuel}})]$ and variance $\hat{W}(s_{\text{fuel}}) := \mathbb{E}[(w(s_{\text{fuel}}) - \hat{w}(s_{\text{fuel}})) \cdot (w(s_{\text{fuel}}) - \hat{w}(s_{\text{fuel}}))^{\top}]$. In this study, the correlation between output variable $w_i(s_{\text{fuel}})$ and $w_j(s_{\text{fuel}}) \forall i, j \in \{1, 2, \dots, n_{\text{PC}}\}$ will be neglected (i.e., $\hat{W}(s_{\text{fuel}})$ is a diagonal matrix), since most literature on GPR assumes the output variables to be uncorrelated. This might affect the quality of the prediction of the cycle-to-cycle variation.

To improve the accuracy of prediction and the determination of hyperparameters, normalised in-cylinder conditions \bar{s}_{fuel} and weights $\bar{w}_i(\bar{s}_{\text{fuel}}^*)$ will be used. Scaling the in-cylinder condition uses the mean $\bar{\mu}_{s_{\text{fuel}},j}^*$ and standard deviation $\bar{\sigma}_{s_{\text{fuel}},j}^*$ of the j th in-cylinder condition variable over the full training set \mathcal{S}^* as

$$\bar{s}_{\text{fuel},j} = \frac{s_{\text{fuel},j} - \bar{\mu}_{s_{\text{fuel}},j}^*}{\bar{\sigma}_{s_{\text{fuel}},j}^*}. \quad (21)$$

The scaling of the weights uses the mean $\bar{\mu}_{w_i}$ and standard deviation $\bar{\sigma}_{w_i}^*$ of the i th in-cylinder conditions variable over the full training set \mathcal{S}^* as

$$\bar{w}_i(\bar{s}_{\text{fuel}}^*) = \frac{w_i(\bar{s}_{\text{fuel}}^*) - \bar{\mu}_{w_i}}{\bar{\sigma}_{w_i}^*}. \quad (22)$$

Following Rasmussen and Williams (2006), the scaled expected value and scaled covariance matrix without correlation can be computed as:

$$\begin{aligned} \hat{w}_i(\bar{s}_{\text{fuel}}) &= K(\bar{s}_{\text{fuel}}, \bar{s}_{\text{fuel}}^*, \phi) \cdot \\ &\quad \left(K(\bar{s}_{\text{fuel}}^*, \bar{s}_{\text{fuel}}^*, \phi) + \bar{W}(\bar{s}_{\text{fuel}}^*) \right)^{-1} \bar{w}_i(\bar{s}_{\text{fuel}}^*) \end{aligned} \quad (23)$$

and

$$\begin{aligned} \hat{W}_{ii}(\bar{s}_{\text{fuel}}) &= K(\bar{s}_{\text{fuel}}, \bar{s}_{\text{fuel}}, \phi) - \\ &\quad K(\bar{s}_{\text{fuel}}, \bar{s}_{\text{fuel}}^*, \phi) \left(K(\bar{s}_{\text{fuel}}^*, \bar{s}_{\text{fuel}}^*, \phi) + \bar{W}(\bar{s}_{\text{fuel}}^*) \right)^{-1} \cdot \\ &\quad K^{\top}(\bar{s}_{\text{fuel}}, \bar{s}_{\text{fuel}}^*, \phi), \end{aligned} \quad (24)$$

where $K(\cdot, \cdot, \phi)$ is the Matérn kernel with $\nu = \frac{2}{3}$ and $\phi = \{\varphi_f, \Phi_1\}$ are the kernel's hyperparameters. The elements in the kernel are given by

$$\begin{aligned} k(x, y, \phi) &= \varphi_f^2 \left(1 + \sqrt{3}\rho(x, y) \right) \cdot \\ &\quad \exp\left(-\sqrt{3}\rho(x, y)\right) \end{aligned} \quad (25)$$

with

$$\rho(x, y) = \sqrt{(x - y)^\top \Phi_1^{-2} (x - y)}. \quad (26)$$

For more information on the selection of the kernel and hyper-parameters, the interested reader is referred to Vlaswinkel and Willems (2024).

Finally, the scaled expected value and scaled covariance matrix are descaled to complete the description of (20). The descaled expected value is given by

$$\hat{w}_i(\bar{s}_{\text{fuel}}) = \hat{\hat{w}}_i(\bar{s}_{\text{fuel}}) \bar{\sigma}_{w_i} + \bar{\mu}_{w_i} \quad (27)$$

and the descaled covariance matrix is given by

$$\hat{W}_{ii}(\bar{s}_{\text{fuel}}) = \hat{\hat{W}}_{ii}(\bar{s}_{\text{fuel}}) \bar{\sigma}_{w_i}. \quad (28)$$

3.4 Predicted Cost and Constraint Violation

Given the PCD of the in-cylinder pressure in Section 3.1, the introduced cost function J_{ITC} associated with energy loss in Section 3.2, and the GPR prediction model in Section 3.3, we can rewrite the optimization problem (6) in terms of PCs $f(\theta)$ and weights $w(s_{\text{fuel}})$. Substituting (7) in (6) results in the following formulation of the engine optimization problem:

$$s_{\text{fuel}}^* = \arg \max_{s_{\text{fuel}} \in \mathcal{S}_{\text{fuel}}} -J_{\text{ITC}}(s_{\text{fuel}}, s_{\text{air}}), \quad (29a)$$

$$\text{s.t. } \hat{w}(s_{\text{fuel}})^\top \int_{\Theta} f(\theta) dV(\theta) = \text{IMEP}_{\text{g,req}}, \quad (29b)$$

$$\text{cov}(\text{IMEP}_{\text{g}}(s_{\text{fuel}}, s_{\text{air}})) < \left[\text{cov}(\text{IMEP}_{\text{g}}(s_{\text{fuel}}, s_{\text{air}})) \right]_{\text{ub}}, \quad (29c)$$

$$p_{\text{mot}}(\theta, p_{\text{im}}) + \hat{w}(s_{\text{fuel}})^\top f(\theta) < p_{\text{ub}} \quad \forall \theta \in \Theta, \quad (29d)$$

$$\left. \frac{\partial p_{\text{mot}}}{\partial \theta} \right|_{\theta} + \hat{w}(s_{\text{fuel}})^\top \left. \frac{df}{d\theta} \right|_{\theta} < dp_{\text{ub}} \quad \forall \theta \in \Theta. \quad (29e)$$

Using the GPR model presented in Section 3.3, the predicted mean and variance of the parameters in (29) can be determined. The required derivations will be presented in the following sections.

3.5 Acquisition Function

At the start of the optimization procedure, the cost function $J_{\text{ITC}}(s_{\text{fuel}}, s_{\text{air}})$ in (29a) is unknown. It is only possible to construct an estimate of the cost function given the previous observations up to time k of collected in the set \mathcal{D}_k . The set \mathcal{D}_k contains the applied s_{fuel} , corresponding observed $w(s_{\text{fuel}})$ and the best observed cost $J_{\text{ITC},k}^*$ until time k . This description also includes uncertainty as a result from cycle-to-cycle behaviour and model uncertainty as a result of cycle-to-cycle variations and measurement noise. The acquisition function is a method of summarising the predicted cost and uncertainty into a scalar function. The acquisition function is used to drive the optimization.

The improvement of the cost is used as a measure to guide the optimization. The improvement at a point s_{fuel} is defined as

(Garnett, 2023, Ch. 7 and 8):

$$I(s_{\text{fuel}} | \mathcal{D}_k) = \max \left(J_{\text{ITC}}(s_{\text{fuel}} | \mathcal{D}_k) - J_{\text{ITC},k}^*, 0 \right), \quad (30)$$

where $J_{\text{ITC}}(s_{\text{fuel}} | \mathcal{D}_k)$ is the mean predicted cost at s_{fuel} given all information collected up to time k denoted with set \mathcal{D}_k and $J_{\text{ITC},k}^*$ is the best observed cost until time k . When the predicted cost is lower compared the best observed cost the improvement is equal to zero. Otherwise, the improvement is equal to the difference between the predicted and best observed cost. In this study, the two most common methods of using the improvement will be discussed: (1) Expected Improvement (EI) and (2) Probability of Improvement (PI). Both are formulated below for the case of noiseless as well as noisy observations.

3.5.1 Expected Improvement

The EI maximizes the expected value of the improvement defined in (30). The general formulation for the EI is given by:

$$\alpha_{\text{EI}}(s_{\text{fuel}} | \mathcal{D}_k) = \mathbb{E} [I(s_{\text{fuel}} | \mathcal{D}_k)]. \quad (31)$$

In the case of noiseless observations this boils down to:

$$\alpha_{\text{EI}}(s_{\text{fuel}} | \mathcal{D}_k) = \int_0^\infty \left[\max(\tau - J_{\text{ITC},k}^*, 0) \cdot g_{\tilde{\chi}^2}(\tau | s_{\text{fuel}}, \mathcal{D}_k) \right] d\tau, \quad (32)$$

where $g_{\tilde{\chi}^2} : \mathbb{R}_{\geq 0} \rightarrow (0, 1)$ is the probability density function for a generalized chi-squared distribution. Using (17), this distribution is parametrized as follows:

$$J_{\text{ITC}}(s_{\text{fuel}}) = w(s_{\text{fuel}})^\top Q_1 w(s_{\text{fuel}}) + q_2 w(s_{\text{fuel}}) + q_0 \quad (33)$$

with $Q_2 = Z_1$, $q_1 = -2w_{\text{ITC}}^\top Z_1 w(s_{\text{fuel}})$ and $q_0 = w_{\text{ITC}}^\top Z_1 w_{\text{ITC}}$. The mean and variance of the normal distributed $w(s_{\text{fuel}})$ are computed using the model described in Section 3.3.

When the observations are noisy, (31) becomes:

$$\alpha_{\text{EI-NO}}(s_{\text{fuel}} | \mathcal{D}_k) = \int_0^\infty \left[g_{\tilde{\chi}^2}(\tau^* | s_{\text{fuel},k}^*, \mathcal{D}_k) \cdot \int_0^\infty [\max(\tau - \tau^*, 0) g_{\tilde{\chi}^2}(\tau | s_{\text{fuel}}, \mathcal{D}_k)] d\tau \right] d\tau^*, \quad (34)$$

here τ^* replaces $J_{\text{ITC},k}^*$ in the original definition of α_{EI} in (32) and $s_{\text{fuel},k}^*$ are the fuel conditions that realized the best observed cost until time k . The probability distribution related to the cost at $s_{\text{fuel},k}^*$ is computed using (33).

3.5.2 Probability of Improvement

The PI maximizes the probability of improving the system. The general formulation for the PI is given by:

$$\alpha_{\text{PI}}(s_{\text{fuel}} | \mathcal{D}_k) = \Pr \left(J_{\text{ITC}}(s_{\text{fuel}} | \mathcal{D}_k) > J_{\text{ITC},k}^* | \mathcal{D}_k \right). \quad (35)$$

In the case of noiseless observations this boils down to:

$$\alpha_{\text{PI}}(s_{\text{fuel}} | \mathcal{D}_k, J_{\text{ITC},k}^*) = 1 - G_{\tilde{\chi}^2} \left(J_{\text{ITC},k}^* | s_{\text{fuel}}, \mathcal{D}_k \right), \quad (36)$$

where $G_{\tilde{\chi}^2} : \mathbb{R}_{\geq 0} \rightarrow (0, 1)$ is the cumulative distribution function for a generalized chi-squared distribution parametrized according to (33) and the model presented in Section 3.3.

When the observations are noisy, (35) becomes:

$$\alpha_{\text{PI-NO}}(s_{\text{fuel}} | \mathcal{D}_k) = \int_0^\infty g_{\tilde{\chi}^2}(\tau^* | s_{\text{fuel}}^*, \mathcal{D}_k) \cdot (1 - G_{\tilde{\chi}^2}(\tau^* | s_{\text{fuel}}^*, \mathcal{D}_k)) d\tau^*, \quad (37)$$

where τ^* replaces $J_{\text{ITC},k}^*$ in the original definition of α_{PI} in (36).

3.6 Constraint Handling

Similar to Gelbart et al. (2014), a probabilistic view of the constraints will be used. The predicted probability of violating the constraints can be computed as non-independent events of violating each individual constraint. Given an input s_{fuel} , the predicted probability of violating each individual constraint is

$$\tilde{\beta}_i(s_{\text{fuel},k}) = \Pr(h_i(s_{\text{fuel},k}) > 0 | s_{\text{fuel},k} \text{ and } \mathcal{D}_k), \quad (38)$$

where $h_i(s_{\text{fuel},k})$ with $i \in \{1, 2, \dots, 4\}$ are a reformulation of the constraints in (29b) to (29e). The reformulation for each constrained is discussed below. The probability $\beta_{n_{\text{const}}}$ of violating the constraints, where n_{const} is the number of constraints, can be recursively solved using

$$\beta_i(s_{\text{fuel},k}) = \beta_{i-1}(s_{\text{fuel},k})(1 - \tilde{\beta}_i(s_{\text{fuel},k})) + \tilde{\beta}_i(s_{\text{fuel},k}) \quad (39)$$

with $i \in \{0, 1, \dots, n_{\text{const}}\}$ and $\beta_0(s_{\text{fuel},k}) = 0$. A $s_{\text{fuel},k}$ will be labelled as infeasible if the probability of violating the constraints exceeds 5%. This limit can be increased to allow for more risky behaviour or decreased to be more risk averse.

It is assumed that the probability distribution of each constraint can be represented with a Gaussian probability distribution. To compute $\tilde{\beta}_i(s_{\text{fuel},k})$ the mean and variance of each constraint is required. This is computed using the current system knowledge \mathcal{D}_k .

3.6.1 IMEP_g Constraint

The constraint related to IMEP_g and cov(IMEP_g) are given in (29b) and (29c), respectively. Given the feedback controller regulating Q_{fuel} to reach IMEP_{g,req} satisfies (29b) if IMEP_{g,req} is reachable at the current BR and SOI_{DI}. The reachability of IMEP_{g,req} and the constraint of (29c) are combined as a constraint for the lower and upper bound on IMEP_g. The lower bound is given by

$$h_1(s_{\text{fuel},k}) = w(s_{\text{fuel},k}) \int_{-180^\circ}^{180^\circ} f(\theta) dV(\theta) - \text{IMEP}_{\text{g,req}} \left(1 - \frac{1}{2} [\text{cov}(\text{IMEP}_{\text{g}})]_{\text{ub}}\right) \quad (40)$$

with $[\text{cov}(\text{IMEP}_{\text{g}})]_{\text{ub}}$ to upper bound of the coefficient of variation on IMEP_g. In this work, $[\text{cov}(\text{IMEP}_{\text{g}})]_{\text{ub}}$ is set to 5%. Using the GPR model presented in Section 3.3, the mean and variance for the lower bound can be predicted using, respectively:

$$\begin{aligned} \mu_{h_1}(s_{\text{fuel},k} | \mathcal{D}_k) &= \\ \hat{w}(s_{\text{fuel},k} | \mathcal{D}_k)^\top \int_{-180^\circ}^{180^\circ} f(\theta) dV(\theta) - & \quad (41) \\ \text{IMEP}_{\text{g,req}} \left(1 - \frac{1}{2} [\text{cov}(\text{IMEP}_{\text{g}})]_{\text{ub}}\right) & \end{aligned}$$

and

$$\begin{aligned} \sigma_{h_1}^2(s_{\text{fuel},k} | \mathcal{D}_k) &= \\ \left(\int_{-180^\circ}^{180^\circ} f(\theta) dV(\theta) \right)^\top \hat{W}(s_{\text{fuel},k} | \mathcal{D}_k) \cdot & \quad (42) \\ \left(\int_{-180^\circ}^{180^\circ} f(\theta) dV(\theta) \right). & \end{aligned}$$

The upper bound is given by

$$\begin{aligned} h_2(s_{\text{fuel},k}) &= w(s_{\text{fuel},k}) \int_{-180^\circ}^{180^\circ} f(\theta) dV(\theta) - \\ \text{IMEP}_{\text{g,req}} \left(1 + \frac{1}{2} [\text{cov}(\text{IMEP}_{\text{g}})]_{\text{ub}}\right). & \quad (43) \end{aligned}$$

The mean and variance for the upper bound are computed as

$$\begin{aligned} \mu_{h_2}(s_{\text{fuel},k} | \mathcal{D}_k) &= \\ -\hat{w}(s_{\text{fuel},k} | \mathcal{D}_k)^\top \int_{-180^\circ}^{180^\circ} f(\theta) dV(\theta) + & \quad (44) \\ \text{IMEP}_{\text{g,req}} \left(1 + \frac{1}{2} [\text{cov}(\text{IMEP}_{\text{g}})]_{\text{ub}}\right) & \end{aligned}$$

and

$$\sigma_{h_2}^2(s_{\text{fuel},k} | \mathcal{D}_k) = \sigma_{h_1}^2(s_{\text{fuel},k} | \mathcal{D}_k), \quad (45)$$

respectively.

3.6.2 Safety Constraints

The safety constraint dealing with $\max_{\theta \in \Theta}(p(\theta, s_{\text{fuel}}))$ and $\max_{\theta \in \Theta} \left(\frac{\partial p}{\partial \theta} \Big|_{\theta, s_{\text{fuel}}} \right)$ are given in (29d) and (29e), respectively. The constraint in (29d) is evaluated at $\theta_{p_{\text{max}}} = \arg \max_{\theta \in \Theta} (\hat{w}(s_{\text{fuel},k} | \mathcal{D}_k)^\top f(\theta) + p_{\text{mp}}(\theta))$ such that

$$\begin{aligned} h_3(s_{\text{fuel},k}) &= w(s_{\text{fuel},k}) f(\theta_{p_{\text{max}}}) + \\ p_{\text{mp}}(\theta_{p_{\text{max}}}) - p_{\text{ub}}. & \quad (46) \end{aligned}$$

Using the GPR model presented in Section 3.3, the mean and variance are computed as

$$\begin{aligned} \mu_{h_3}(s_{\text{fuel},k} | \mathcal{D}_k) &= \\ \hat{w}(s_{\text{fuel},k} | \mathcal{D}_k)^\top f(\theta_{p_{\text{max}}}) + p_{\text{mp}}(\theta_{p_{\text{max}}}) - p_{\text{ub}} & \quad (47) \end{aligned}$$

and

$$\begin{aligned} \sigma_{h_3}^2(s_{\text{fuel},k} | \mathcal{D}_k) &= \\ f^\top(\theta_{p_{\text{max}}}) \hat{W}_{\hat{w}}(s_{\text{fuel},k} | \mathcal{D}_k) f(\theta_{p_{\text{max}}}). & \quad (48) \end{aligned}$$

The constraint given in (29e) is evaluated at $\theta_{dp_{\text{max}}} = \arg \max_{\theta \in \Theta} (\hat{w}(s_{\text{fuel},k} | \mathcal{D}_k)^\top \frac{df}{d\theta} + \frac{dp_{\text{mp}}}{d\theta})$ such that

$$\begin{aligned} h_4(s_{\text{fuel},k}) &= w(s_{\text{fuel},k}) \frac{df}{d\theta} \Big|_{\theta_{dp_{\text{max}}}} + \\ \frac{dp_{\text{mp}}}{d\theta} \Big|_{\theta_{dp_{\text{max}}}} - dp_{\text{ub}} & \quad (49) \end{aligned}$$

The mean and variance are computed as

$$\begin{aligned} \mu_{h_4}(s_{\text{fuel},k} | \mathcal{D}_k) &= \\ \hat{w}(s_{\text{fuel},k} | \mathcal{D}_k)^\top \frac{df}{d\theta} \Big|_{\theta_{dp_{\text{max}}}} + & \quad (50) \\ \frac{dp_{\text{mp}}}{d\theta} \Big|_{\theta_{dp_{\text{max}}}} - dp_{\text{ub}} & \end{aligned}$$

and

$$\sigma_{h_4}^2(s_{\text{fuel},k} | \mathcal{D}_k) = \left(\frac{df}{d\theta} \Big|_{\theta_{dp_{\max}}} \right)^T \hat{W}_{\hat{w}}(s_{\text{fuel},k} | \mathcal{D}_k) \cdot \left(\frac{df}{d\theta} \Big|_{\theta_{dp_{\max}}} \right). \quad (51)$$

3.7 Particle Swarm Optimisation with Constraints

The BO problem is non-convex and has multiple local optima. PSO is used to find the global optimum of the acquisition function given the system knowledge \mathcal{D}_k . It is performed every iteration of the BO approach and is responsible for selecting the next solution being applied to the system. It uses different candidate solutions that over different iteration ℓ are moving towards the global optimum. Each candidate solution has a cost value, constraint violation probability, position and velocity. The computation of the cost value is discussed in Section 3.5 and the constraint violation probability in Section 3.6. In this section, the updating rules of the position s_{fuel} of the candidate solution is discussed.

Several iterations of the PSO are required to find the global optimum. A single iteration is denoted with $\ell \in \mathbb{N}_0$. The PSO uses n_{PSO} particles. Each particle has a location $\tilde{s}_{\text{fuel}}^i \in \mathcal{S}_{\text{fuel}}$ and velocity $v^i \in \mathbb{R}^2$, where the subscript $i \in \{1, 2, \dots, n_{\text{PSO}}\}$ indicates the specific particle. Each iteration the location of all the particles is update according to

$$\tilde{s}_{\text{fuel},\ell}^i = \tilde{s}_{\text{fuel},\ell-1}^i + v_\ell^i \quad (52)$$

with

$$v_\ell^i = c_0 v_{\ell-1}^i + c_1 X_{1,\ell} (\tilde{s}_{\text{fuel,p,best}}^i - \tilde{s}_{\text{fuel},\ell-1}^i) + c_2 X_{2,\ell} (\tilde{s}_{\text{fuel,g,best}}^i - \tilde{s}_{\text{fuel},\ell-1}^i), \quad (53)$$

where $\tilde{s}_{\text{fuel,p,best}}^i$ is the best observed cost of the i th particle, $\tilde{s}_{\text{fuel,g,best}}^i$ is the best observed cost over all particles, $c_k \in (0, 1)$, $k \in \{1, 2, 3\}$ are tuning parameters and $X_{j,\ell}$, $j \in \{1, 2\}$ are samples taken from the standard uniform distribution. The initial particle locations $\tilde{s}_{\text{fuel},0}^i$ are selected from a uniform distribution spanning the actuator range and initial particle velocities v_0^i are selected from a normal distribution.

A similar approach to select the location of the best cost as Lampinen (2002) will be used. In their work, the following method selects $\tilde{s}_{\text{fuel,p,best}}^i$ and $\tilde{s}_{\text{fuel,g,best}}^i$ as a the best candidate solutions from the whole population when:

- if $\tilde{s}_{\text{fuel},\ell}^i$ is feasible and the value of the objective function gives the largest or equal value of the previous observed costs with a feasible solution, or
- if $\tilde{s}_{\text{fuel},\ell}^i$ is feasible while the other previously observed solutions of the population are infeasible, or
- all solutions in the population are infeasible, but $\tilde{s}_{\text{fuel},\ell}^i$ has the lowest or equal violation of the constraints.

The constrained PSO is summarized in Algorithm 1.

Table 2: Settings for the simulated engine calibration in Section 4 using the method presented in this study.

Parameter	Value
IMEP _{g,ref}	4 bar
Q_{fuel} range	[1639.6, 2405.8] J/cycle
BR range	[0.7046, 0.8188]
BR ₀	0.8
SOI _{DI} range	[-75, -35] CADaTDC
SOI _{DI,0}	-45 CADaTDC
[cov(IMEP _g)] _{ub}	10%
p_{\max}	200 bar
dp_{\max}	25 bar/CAD
n_{sample}	25
n_{PSO}	100
c_0	0.1
c_1	0.01
c_2	0.1

4 RESULTS

In this section, the proposed method is evaluated from simulation results. For the engine described in Section 2, a stochastic RCCI engine model was developed in earlier work. Based on fuelling settings s_{fuel} and air path conditions s_{air} , this engine model provides the in-cylinder pressure trace, including the cycle-to-cycle variation during the compression and expansion stroke. This model was validated using experimental engine data and shows good prediction capabilities. It is further described in Vlaswinkel and Willems (2024).

Using this model, first a brief discussion of the exploration mechanics using α_{EI} is presented. Second, a comparison is made between the four acquisition functions presented in Section 3.5. The initial conditions and settings for the evaluation are given in Table 2. The actuator ranges and IMEP_{g,ref} are chosen to be inline with the simulation model. The bounds on the inequality constraints (p_{\max} , dp_{\max} and [cov(IMEP_g)]_{ub}) are determined by the engine specifications. The parameters n_{sample} and n_{PSO} are determined using a trail-and-error approach. The PSO parameters c_0 , c_1 and c_2 are chosen to prefer a move towards the global optimum.

4.1 Evaluation of Single Acquisition Function

Figure 2 shows the acquisition function and constraint boundaries at different iterations of the BO using α_{NEI} . It shows in Figures 2a until 2c that up to the first 50 iterations the BO is expanding the constraint boundaries. The active constraint is the constraint on IMEP_g and cov(IMEP_g). After 50 iterations the algorithm focusses on refining the information gathered in the area within the constraint bounds as shown in Figures 2d.

The other acquisition functions presented in Section 3.5 show similar patterns. For brevity, they are discussed in A.

4.2 Comparison Between Acquisition Functions

Figures 3 and 4 show important observed parameters and the actuator settings over time for the different acquisition func-

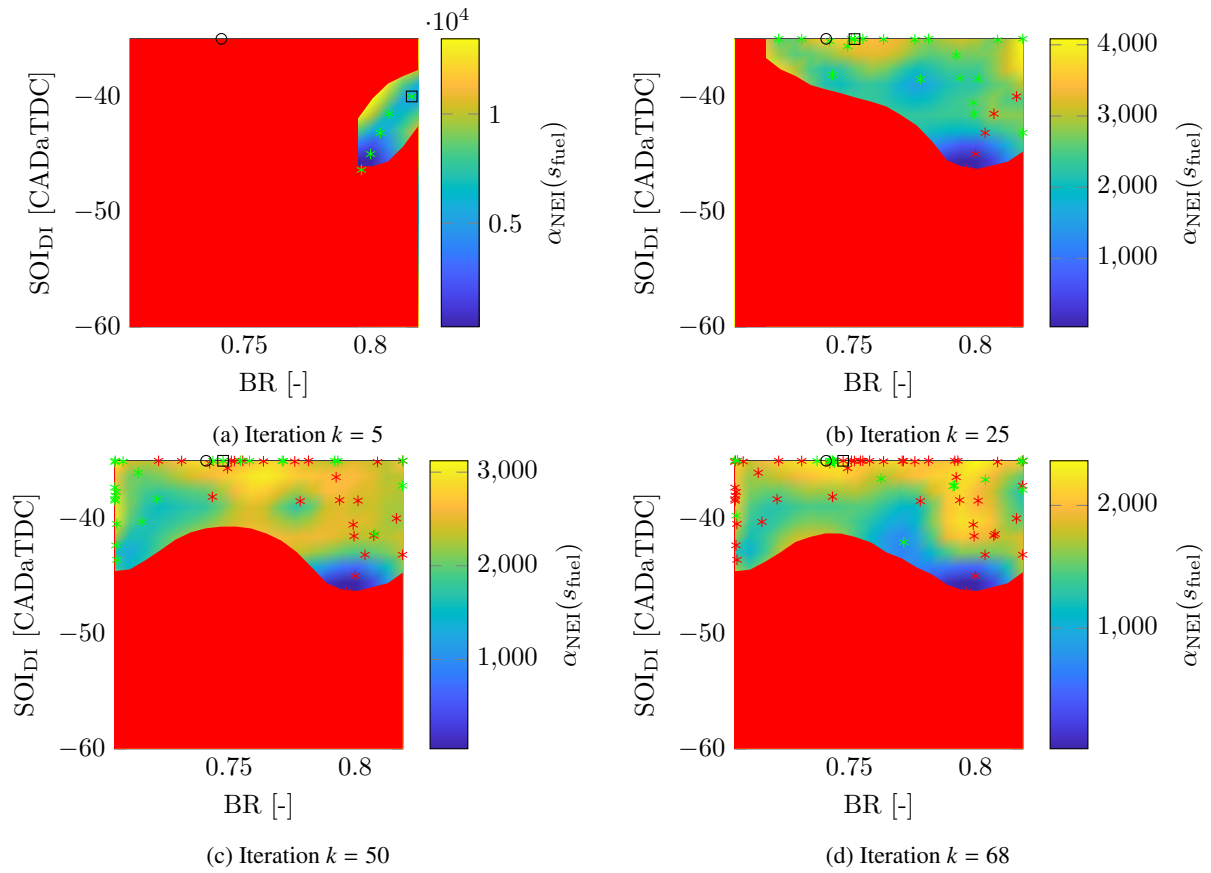


Figure 2: Solving the Bayesian Optimisation using α_{NEI} with default constraint settings. New samples (green), old sample (red); best observed iteration (square), optimum (circle).

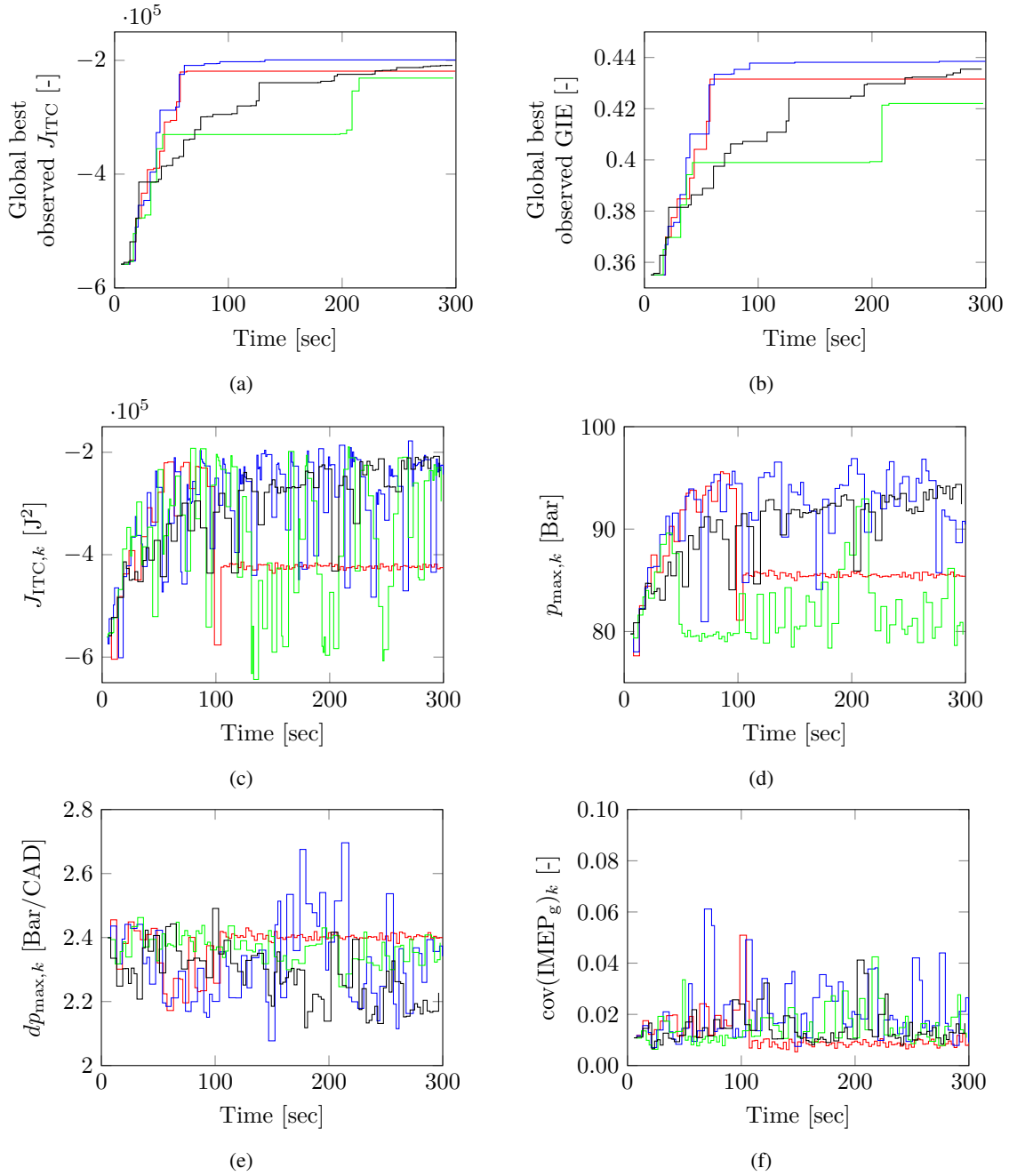


Figure 3: Important observed parameters over time using α_{EI} (red), α_{NEI} (blue), α_{PI} (green) and α_{NPI} (black)

Algorithm 1 Overview of the constrained Particle Swarm Optimizer presented in Section 3.7

```

1:  $\ell \leftarrow 0$ 
2:  $\tilde{s}_{\text{fuel},0} \leftarrow$  Uniform grid of  $n_{\text{PSO}}$  particles spanning  $\mathcal{S}_{\text{fuel}}$ 
3:  $v_0 \leftarrow n_{\text{PSO}}$  randomly generated velocities vectors
4: for  $\ell < 100$  do
5:    $\ell \leftarrow \ell + 1$ 
6:   for all  $\tilde{s}_{\text{fuel},\ell-1}^i \in \tilde{s}_{\text{fuel},\ell-1}$  do
7:      $v_\ell^i \leftarrow (53)$ 
8:      $\tilde{s}_{\text{fuel},\ell}^i \leftarrow (52)$ 
9:      $\alpha(\tilde{s}_{\text{fuel},\ell}^i | \mathcal{D}_k) \leftarrow (32)/(34)/(36)/(37)$ 
10:     $\beta_{n_{\text{const}}}(\tilde{s}_{\text{fuel},\ell}^i | \mathcal{D}_k) \leftarrow (39)$ 
11:    if  $\beta_{n_{\text{const}}}(\tilde{s}_{\text{fuel},\ell}^i) \leq 0.05$  and  $\beta_{n_{\text{const}}}(\tilde{s}_{\text{fuel,p,best}}^i) \leq 0.05$  then ▷ Feasibility checks
12:       $\tilde{s}_{\text{fuel,p,best}}^i \leftarrow \arg \max (\alpha(\tilde{s}_{\text{fuel,p,best}}^i), \alpha(\tilde{s}_{\text{fuel},\ell}^i))$ 
13:    else if  $\beta_{n_{\text{const}}}(\tilde{s}_{\text{fuel},\ell}^i) \leq 0.05$  and  $\beta_{n_{\text{const}}}(\tilde{s}_{\text{fuel,p,best}}^i) > 0.05$  then
14:       $\tilde{s}_{\text{fuel,p,best}}^i \leftarrow \tilde{s}_{\text{fuel},\ell}^i$ 
15:    else
16:       $\tilde{s}_{\text{fuel,p,best}}^i \leftarrow \arg \min (\beta_{n_{\text{const}}}(\tilde{s}_{\text{fuel,p,best}}^i), \beta_{n_{\text{const}}}(\tilde{s}_{\text{fuel},\ell}^i))$ 
17:    end if
18:  end for
19:   $\tilde{s}_{\text{fuel,g,best}} \leftarrow \arg \max (\alpha(\tilde{s}_{\text{fuel,g,best}}), \alpha(\tilde{s}_{\text{fuel,p,best}}))$  ▷ Only use  $\tilde{s}_{\text{fuel},\ell}^i$  with  $\beta_{n_{\text{const}}}(\tilde{s}_{\text{fuel},\ell}^i) \leq 0.05$ 
20: end for
21: Apply  $\tilde{s}_{\text{fuel,g,best}}$  to the system

```

tions presented in Section 3.5. Figures 3a and 3b show the best observed cost J_{ITC} and GIE over time. Figure 3c shows the cost at each iteration of the BO. It can be seen that by using α_{NEI} and α_{NPI} the BO converges towards similar GIE; however, using α_{NPI} takes substantially longer. The acquisition functions α_{EI} and α_{PI} start selecting suboptimal solutions after convergence.

Figure 4 shows the selected BR and SOI_{DI} over time for the demonstrated acquisition functions. Figure 4a shows that α_{PI} and α_{NPI} only explore a small region of the allowed range of BR compared to α_{EI} and α_{NEI} . Figure 4b shows that all demonstrated acquisition functions explore a similar range of SOI_{DI} . The acquisition function α_{NEI} keeps exploring the full operating range within constrained bounds after the optimal solution is found. The acquisition function α_{NPI} tends to prefer selecting the actuator settings close to the current best found solution, hence being more exploiting. After finding the optimum solution α_{EI} and α_{PI} tend to exploit a non-optimal actuator setting.

Figure 3d, 3e and 3f show the values related to the constraints of each iteration. It can be seen that in all cases, the BO respects the constraints. Since the constraints are not part of the acquisition function, no difference between constraint handling is observed.

Table 3 shows a comparison between the four acquisition functions. A comparison is made between the location of the found best solution and the true optimum. Also a comparison is made between the difference in J_{ITC} and GIE at the best found solution and the true optimum. Lastly, the convergence time of each acquisition function is given for the used initial conditions. The convergence time is define as the moment that a new best solution is found, but the improvement in GIE is less than 0.1 % compared to the best found GIE at $t = 300$ s.

The acquisition functions using the expected improvement α_{EI} and α_{NEI} found actuator setpoints that have an GIE less then 0.1 % from the true optimum within 60 s. The acquisition function using the probability of improvement found an ΔGIE of 1.5 % for α_{PI} and 0.4 % for α_{NPI} ; however the convergence time of these acquisition functions is substantially longer compared to α_{EI} and α_{NEI} . The fastest convergence time is achieved with α_{NEI} and the slowest convergence time with α_{PI} .

The acquisition function α_{NEI} is selected as the best option. It finds the true optimum and shows a more exploitive behaviour when the optimum is found and the feasible region is fully explored. Furthermore, a convergence time of 56.8 s is found given the used initial conditions.

5 CONCLUSIONS AND FUTURE RESEARCH

This paper presents an automated, risk-aware calibration method for RCCI engine actuator setpoints. The proposed method uses constrained Bayesian Optimisation (BO) as a probabilistic framework to guide the calibration process. The method does not require prior knowledge about the system and during the calibration process knowledge about the system is collected. Using a previously developed method that predicts the in-cylinder pressure between IVC and EVO the proposed method is able to prevent maximum peak pressures and maximum peak pressure rise-rates that exceed specified bounds.

The proposed method was successfully demonstrate in simulations using a validated RCCI engine model. The method was able to find the optimal fuelling settings within 60 s for the used initial condition and acquisition functions. No constraints were violated during the calibration process. As a result, no unsafe setpoints were applied to the simulated system.

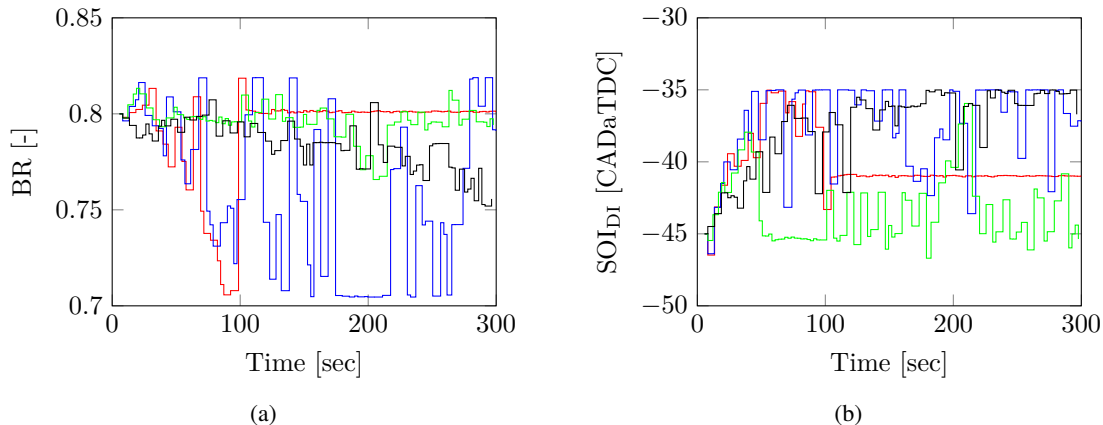
Figure 4: Actuator settings over time using α_{EI} (red), α_{NEI} (blue), α_{PI} (green) and α_{NPI} (black)

Table 3: Overview of the best found solution and performance using the different acquisition function presented in Section 3.5.

Acquisition function	ΔBR [-]	ΔSOI_{D1} [CAD]	ΔJ_{ITC} [J ²]	ΔGIE [-]	Convergence time [s]
α_{EI}	0.020	0.21	1.2×10^3	-8.2×10^{-3}	57.7
α_{NEI}	0.0067	0.0019	7.7×10^2	-9.3×10^{-4}	56.8
α_{PI}	0.0267	0.95	2.4×10^5	-1.5×10^{-2}	208.7
α_{NPI}	0.0139	0.29	1.0×10^3	-4.2×10^{-3}	193.2

In the future, experimental demonstration of the proposed self-learning calibration method is planned. This will require a reduction in the computation time of the algorithm. Furthermore, the algorithm can not handle transient behaviour. This becomes especially important when the algorithm is used in on-road applications, since it will be unlikely that the engine will reach steady-state behavior.

A VISUALISATION OF THE PRESENTED ACQUISITION FUNCTIONS

Figure 5 shows the value of the acquisition function and constraint boundaries at different iterations of the BO using an acquisition function that does not deal with noisy observations α_{EI} . Figures 5a and 5b show that in the first 25 iterations the optimization with α_{EI} explores the constraint boundaries. During this period, the constraint boundary is extended. This increases the feasible operating domain. After the first 25 iterations the optimization with α_{EI} selects one point close to the initial guess as shown in Figures 5c and 5e. The optimization with α_{EI} does not show a tendency to prefer selecting operating points close to the found optimum.

Figure 6 shows the acquisition function and constraint boundaries at different iterations of the BO using α_{PI} . It shows in Figures 6a and 6b that up to the first 25 iterations the BO is expanding the constraint boundaries. The active constraint is the constraint on $IMEP_g$ and $cov(IMEP_g)$. After 25 iterations the algorithm focusses on refining the information gathered in the area within the constraint bounds as shown in Figure 6d. During these iterations, the constrained boundary is extended a little bit, but is not explored fully.

Figure 7 shows the acquisition function and constraint boundaries at different iterations of the BO using α_{NPI} . It shows in Figures 7a until 7d that up to the first 75 iterations the BO is expanding the constraint boundaries. This expanding seems to be slower compared to the other acquisition functions. The active constraint is the constraint on $IMEP_g$ and $cov(IMEP_g)$.

DECLARATION OF COMPETING INTEREST

The authors declare that they have no known competing financial interests or personal relationships that could have appeared to influence the work reported in this paper.

ACKNOWLEDGEMENTS

The research presented in this study is financially supported by the Dutch Technology Foundation (STW) under project number 14927.

REFERENCES

- E. G. Adam B. Dempsey, N. Ryan Walker, R. D. Reitz, Comparison of low temperature combustion strategies for advanced compression ignition engines with a focus on controllability, *Combustion Science and Technology* 186 (2014) 210–241. doi:10.1080/00102202.2013.858137.
- S. L. Kokjohn, R. M. Hanson, D. A. Splitter, R. D. Reitz, Fuel reactivity controlled compression ignition (rci): a pathway to controlled high-efficiency clean combustion, *International Journal of Engine Research* 12 (2011) 209–226. doi:10.1177/1468087411401548.

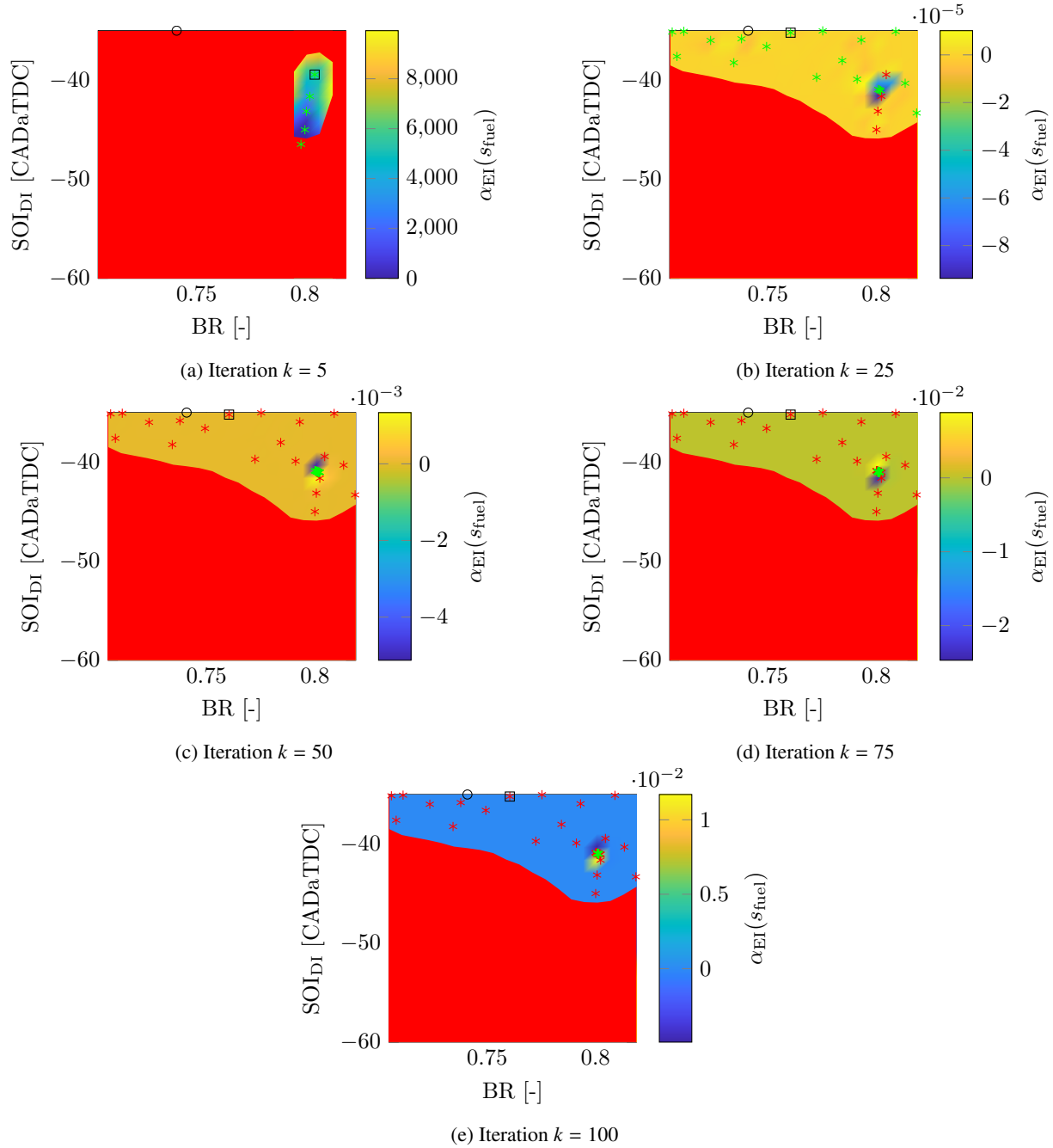


Figure 5: Solving the Bayesian Optimisation using α_{EI} with default constraint settings. New samples (green), old sample (red); best observed iteration (square), optimum (circle).

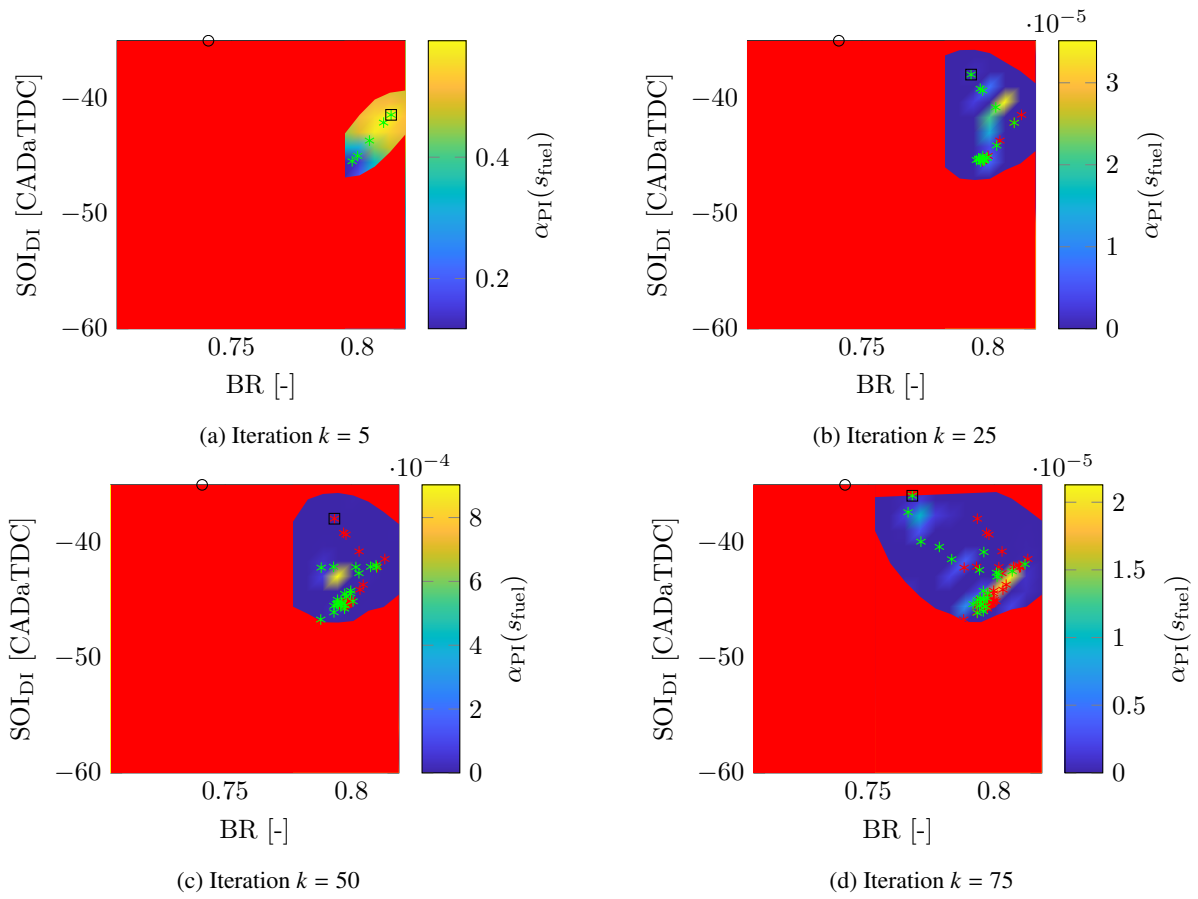


Figure 6: Solving the Bayesian Optimisation using α_{PI} with default constraint settings. New samples (green), old sample (red); best observed iteration (square), optimum (circle).

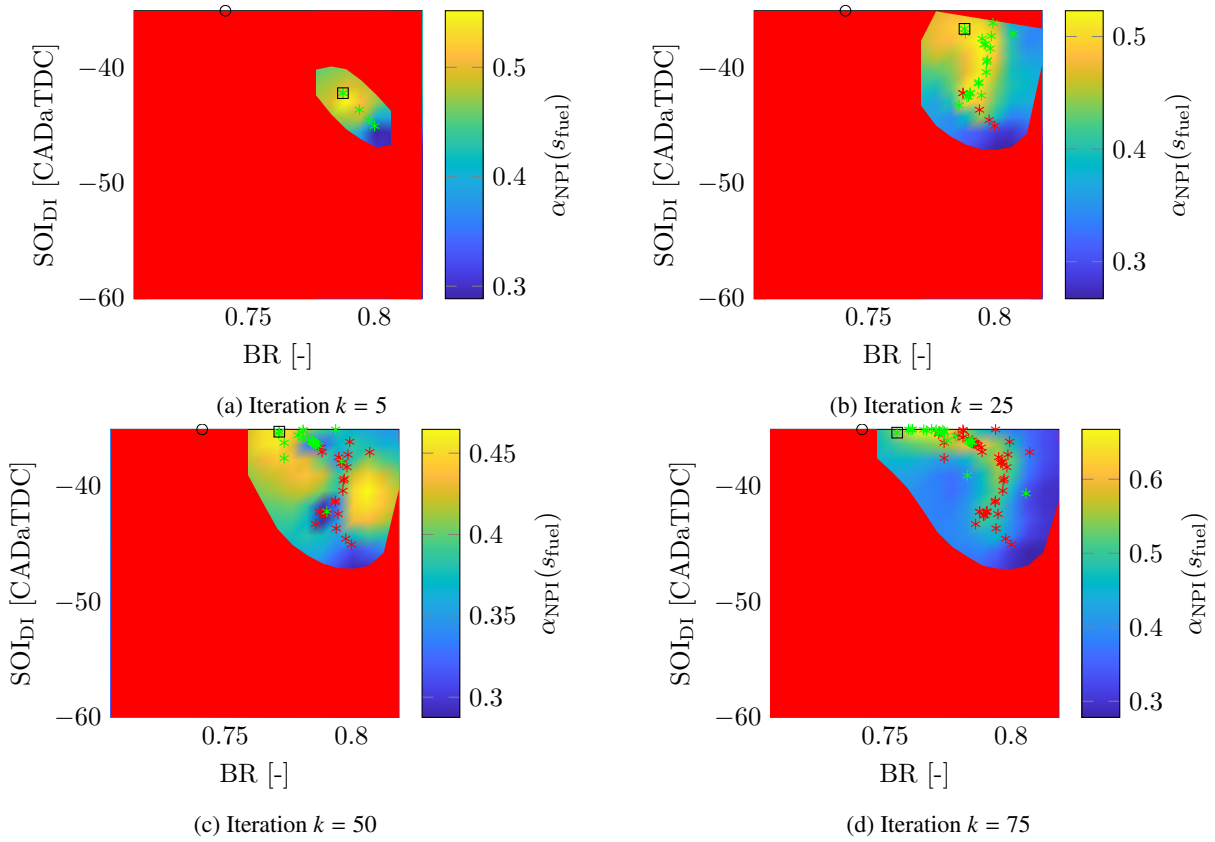


Figure 7: Solving the Bayesian Optimisation using α_{NPI} with default constraint settings. New samples (green), old sample (red); best observed iteration (square), optimum (circle).

- F. Willems, Is cylinder pressure-based control required to meet future hd legislation?, *IFAC-PapersOnLine* 51 (2018) 111–118. doi:<https://doi.org/10.1016/j.ifacol.2018.10.021>, 5th IFAC Conference on Engine and Powertrain Control, Simulation and Modeling E-COSM 2018.
- A. Norouzi, H. Heidarifar, M. Shahbakhti, C. R. Koch, H. Borhan, Model predictive control of internal combustion engines: A review and future directions, *Energies* 14 (2021). doi:10.3390/en14196251.
- A. Paykani, A. Garcia, M. Shahbakhti, P. Rahnama, R. D. Reitz, Reactivity controlled compression ignition engine: Pathways towards commercial viability, *Applied Energy* 282 (2021) 116174. doi:<https://doi.org/10.1016/j.apenergy.2020.116174>.
- S. Grasreiner, J. Neumann, M. Wensing, C. Hasse, Model-based virtual engine calibration with the help of phenomenological methods for spark-ignited engines, *Applied Thermal Engineering* 121 (2017) 190–199. doi:<https://doi.org/10.1016/j.applthermaleng.2017.04.046>.
- T. Y. Motlagh, L. N. Azadani, K. Yazdani, Multi-objective optimization of diesel injection parameters in a natural gas/diesel reactivity controlled compression ignition engine, *Applied Energy* 279 (2020) 115746. doi:<https://doi.org/10.1016/j.apenergy.2020.115746>.
- L. Xia, B. de Jager, T. Donkers, F. Willems, Robust constrained optimization for rcci engines using nested penalized particle swarm, *Control Engineering Practice* 99 (2020) 104411. doi:<https://doi.org/10.1016/j.conengprac.2020.104411>.
- R. Willems, F. Willems, N. Deen, B. Somers, Heat release rate shaping for optimal gross indicated efficiency in a heavy-duty rcci engine fueled with e85 and diesel, *Fuel* 288 (2021) 119656. doi:<https://doi.org/10.1016/j.fuel.2020.119656>.
- S. Biswas, D. Kakati, P. Chakraborti, R. Banerjee, Performance-emission-stability mapping of ci engine in rcci-pcci modes under varying ethanol and cng induced reactivity profiles: A comparative study through experimental and optimization perspectives, *Energy* 254 (2022) 124231. doi:<https://doi.org/10.1016/j.energy.2022.124231>.
- J. Moradi, A. Gharehghani, M. Aghahasani, Application of machine learning to optimize the combustion characteristics of rcci engine over wide load range, *Fuel* 324 (2022) 124494. doi:<https://doi.org/10.1016/j.fuel.2022.124494>.
- S. Greenhill, S. Rana, S. Gupta, P. Vellanki, S. Venkatesh, Bayesian optimization for adaptive experimental design: A review, *IEEE Access* 8 (2020) 13937–13948. doi:10.1109/ACCESS.2020.2966228.
- M. Vlaswinkel, F. Willems, Data-based in-cylinder pressure model with cyclic variations for combustion control: An RCCI engine application, *Energies* 17 (2024). doi:10.3390/en17081881.
- M. Vlaswinkel, F. Willems, Cylinder pressure feedback control for ideal thermodynamic cycle tracking: Towards self-learning engines, *IFAC-PapersOnLine* 56 (2023) 8260–8265. doi:<https://doi.org/10.1016/j.ifacol.2023.10.1011>, 22nd IFAC World Congress.
- J. B. Heywood, *Internal Combustion Engine Fundamentals*, Second Edition, McGraw-Hill Education, 2018.
- C. E. Rasmussen, C. K. I. Williams, *Gaussian Processes for Machine Learning*, MIT Press, 2006.
- R. Garnett, *Bayesian Optimization*, Cambridge University Press, 2023.
- M. A. Gelbart, J. Snoek, R. P. Adams, Bayesian optimization with unknown constraints, 2014. URL: <https://arxiv.org/abs/1403.5607>.
- J. Lampinen, A constraint handling approach for the differential evolution algorithm, in: *Proceedings of the 2002 Congress on Evolutionary Computation. CEC'02 (Cat. No.02TH8600)*, volume 2, 2002, pp. 1468–1473 vol.2. doi:10.1109/CEC.2002.1004459.